Inorg. Chem. **2008**, *47*, 9248−9255

Dimolybdenum Bis-2,4,6-triisopropyl-benzoate Bis-4-isonicotinate: A Redox Active Analogue of 4,4′-Bipyridine with Ambivalent Properties

Malcolm H. Chisholm,*,† Angela S. Dann,† Fabian Dielmann,§ Judith C. Gallucci,† Nathan J. Patmore,*,‡ Ramkrishna Ramnauth,† and Manfred Scheer*,§

Department of Chemistry, The Ohio State University, Columbus, Ohio 43210, Universität Regensburg, Regensburg, Germany, and Sheffield University, Sheffield S3 7HF, England

Received April 17, 2008

The reaction between $Mo_2(TiPB)_4$ and 4-iso-nicotinic acid (2 equiv) in ethanol leads to the formation of *trans*-$Mo_2(TiPB)_2(nic)_2$, **I**, where TiPB = 2,4,6-triisopropylbenzoate and nic = 4-isonicotinate. The molecular structures of **I** and **I**·2DMSO were determined in the solid state by a single-crystal X-ray study, and its electronic structure was determined by DFT calculations on a model compound, where formate ligands were substituted for the bulky TiPB. The physicochemical properties of **I** are reported, and its potential as a redox active building block, a quasi-metalloorganic analogue of 4,4′-bipyridine, is described in the synthesis of molecular and solid-state assemblies. The molecular structure of **I** in the solid state consists of a 3-dimensional network in which each unit of $Mo_2(TiPB)_2(nic)_2$ acts as a donor and acceptor via N to Mo coordination. In the structure of **I**·2DMSO, the DMSO ligands coordinate axially with the Mo−Mo bond via oxygen. The reaction between **I** and $Rh_2(O_2CMe)_4$ is shown to give a 1-D polymeric chain in the solid state: $[\{Rh_2(O_2CMe)_4\}\{Mo_2(TiPB)_2(nic)_2\}]_\infty$, **II**. A similar structure was found for the product involving $Rh_2(O_2CCMe_3)_4$. Evidence is also reported for the formation of $[(1,5\text{-COD})MePt]_2[\mu\text{-}Mo_2(TiPB)_2(nic)_2](PF_6)_2$, **III**, and $[(1,5\text{-COD})Pt(\mu\text{-}\mathbf{I})(PF_6)_2]_n$.

Introduction

The self-assembly of metallo-organic nanoscale molecular species and metalloorganic framework porous solids employs the use of metal ions and bridging ligands with well-specified architectural requirements. The principles of this type of geometric construction have been well articulated and executed by the pioneering work of Stang[1−3] and O'Keeffe and Yaghi[4,5] and their respective groups. A common building block is a linear bifunctional molecule such as the neutral 4,4′-bipyridine molecule or the anionic (2−) 1,4-terephthalate. A recent interest in the Chisholm group has been developing the principles of electronic communication between M_2 quadruply bonded units linked by organic π-systems.[6,7] As an extension of this work, we became interested in how M_2 units could be modified to form redox active building blocks in the assembly of higher-order molecular and solid-state systems. We describe here the preparation and use of a redox active Mo_2 unit that behaves as an enlarged metalloorganic analogue of the neutral 4,4′-bipyridine. This compound behaves both as an acceptor and a donor. During the course of this work, Cotton and Murillo reported a related Mo_2^{4+}-containing unit that acts as a cis-templating agent.[8] This work in turn followed that of Dunbar et al., who prepared a mixed metal square $[cis\text{-}Re_2(\mu\text{-nic})_2Cl_2(\mu\text{-dppm})_2Pt(PEt_3)_2]_2(O_3SCF_3)_4$.[9]

Results and Discussion

Synthesis of *trans*-$Mo_2(TiPB)_2(nic)_2$, I. The reaction between $Mo_2(TiPB)_4$ (TiPB = 2,4,6-triisopropylbenzoate)

* To whom correspondence should be addressed. E-mail: chisholm@chemistry.ohio-state.edu (M.H.C.), n.patmore@sheffield.ac.uk (N.J.P.), manfred.scheer@chemie.uni-regensberg.de (M.S.).
† The Ohio State University.
‡ Sheffield University.
§ Universität Regensburg.

(1) Olenyuk, B.; Whiteford, J. A.; Shield, J. E.; Stang, P. J. *Nature* **1999**, *398*, 796.
(2) Olenyuk, B.; Leininger, S.; Stang, P. J. *Chem. Rev.* **2000**, *100*, 853.
(3) Seidel, S. R.; Stang, P. J. *Acc. Chem. Res.* **2002**, *35*, 972.
(4) Ockwig, N.; Friedrichs, O. D.; O'Keefe, M.; Yaghi, O. M. *Acc. Chem. Res.* **2005**, *38*, 176.
(5) Eddaoudi, M.; Moler, D.; Li, H.; Reineke, T. M.; O'Keefe, M.; Yaghi, O. M. *Acc. Chem. Res.* **2001**, *34*, 319.
(6) Chisholm, M. H.; Patmore, N. J. *Acc. Chem. Res.* **2007**, *40*, 19.
(7) Chisholm, M. H. *Proc. Nat. Acad. Sci. U.S.A.* **2007**, *104*, 2563.
(8) Cotton, F. A.; Jin, J.-Y.; Li, Z.; Liu, C. Y.; Murillo, C. A. *Dalton Trans.* **2007**, 2328.
(9) Bera, J. K.; Smucker, B. W.; Walton, R. A.; Dunbar, K. R. *Chem. Commun.* **2001**, 2565.

10.1021/ic800693r CCC: $40.75
Published on Web 09/26/2008

and 4-isonicotinamic acid (2 equiv) in ethanol leads to the formation of the title compound *trans*-$Mo_2(TiPB)_2(nic)_2$, **I** (nic = 4-isonicotinate). Compound **I** is a red solid that is insoluble in toluene and other hydrocarbon solvents. In general, $Mo_2(O_2CR)_4$ compounds are known to form laddered structures in the solid state as a result of weak intermolecular carboxylate oxygen to molybdenum bonds along the MM axis.[10,11] In the case of $Mo_2(TiPB)_2(nic)_2$, the 4-isonicotinate ligands can act as ligands to the Mo_2^{4+} center, and crystals of **I** were found to have a 3-dimensional network structure. In the space group *I*41/*a*, there are 8 molecules in the unit cell which are related by symmetry. Only one-half of the discrete molecule is uniquely defined crystallographically. Two views of the molecular packing are shown in Figure 1. Viewed along the *c* axis, one can see that the network consists of fused molecular squares. In Figure 2, we show the number atom scheme and full details of bond lengths and angles are given in the Supporting Information. The Mo−Mo distance of 2.1106(4) Å and the Mo−O distances to the carboxylate groups 2.10(1) Å (av) are unexceptional. The Mo−N distance of 2.523(4) Å is long but again not exceptional for axial ligation to the Mo_2^{4+} center.[10]

Molecular Structure of I·2DMSO. Crystals of **I**·2DMSO suitable for an X-ray study were obtained by crystallization from the donor solvent DMSO. In the space group $P\bar{1}$ the molecule has a crystallographically imposed inversion center, and the dinuclear unit has weak axial coordination by DMSO molecules Mo···O(5) = 2.490(3) Å. An ORTEP drawing of the molecule is shown in Figure 3. The geometry of the central $Mo_2(O_2C)_4$ unit is typical of those seen in numerous $Mo_2(O_2CR)_4$ compounds[10] and is akin to the central unit described above. The bulky 2,4,6-triisopropylbenzoates are mutually trans, and the aryl C_6 ring is twisted close to 90° from the O_2C carboxylate plane. This removes $Mo_2\delta$ to benzoate π-conjugation. In contrast, the 4-isonicotinate ligands are oriented in a planar conformation to maximize L−Mo_2−L π-conjugation, as indeed they are in the structure of the extended network structure described above.

[{$Rh_2(O_2CMe)_4$}{$Mo_2(TiPB)_2(nic)_2$}]$_\infty$, II. When blue-green solutions of $Rh_2(O_2CMe)_4$ are allowed to react with orange solutions of **I** in THF, an orange microcrystalline solid is formed. By allowing the two species to react via diffusion in THF and acetonitrile solutions, clear orange-red crystals of the 1:1 adduct [{$Rh_2(O_2CMe)_4$}{$Mo_2(TiPB)_2(nic)_2$}]$_\infty$ (compound **II**) suitable for a crystallographic study were obtained. In the solid state, compound **II** exists as an infinite chain polymer, where **I** acts as a linear bridging ligand. A view of a section of the one-dimensional chain of **II** is shown in Figure 4.

The molecular unit of **I** within the chain of **II** is remarkably similar, in both its dimensions and conformation, to that seen in the discrete molecule shown in Figure 3. The isonicotinate ligands are essentially planar allowing Lπ−$Mo_2\delta$−Lπ conjugation, although the axial ligation of the pyridine ligands to the Rh_2^{4+} unit is not expected to lead to any long-range electronic communication along the chain, vide infra. Each bridging Mo_2^{4+} unit is also ligated by THF molecules along the Mo−Mo axis. These substitute for the DMSO molecules seen in the structure of **I**, shown in Figure 3. Selected bond distances and bond angles are given in Table 1.

A similar 1:1 product was obtained in the reaction between $Rh_2(O_2CCMe_3)_4$ and $Mo_2(TiPB)_2(nic)_2$, whose structure differs little from that of **II** noted above except for the orientation of the C_6 planes of the TiPB ligands. This molecular structure is compared in the Supporting Information.

[(1,5-COD)PtMe]$_2${μ-$Mo_2(TiPB)_2(nic)_2$}$(PF_6)_2$, III. In an attempt to prepare a discrete complex containing the bridging unit, **I**, we prepared (1,5-COD)PtMeCl (COD = cyclooctadiene) according to the reaction sequence shown in Scheme 1.[12]

Then, by reaction with $AgPF_6$ in acetone, the labile cation (1,5-COD)PtMe(acetone)$^+$ was prepared. This was reacted with **I** in the ratio 2:1, with the aim of forming [(1,5-COD)PtMe]$_2$[μ-$Mo_2(TiPB)_2(nic)_2$]$(PF_6)_2$, **III**. The formation of (1,5-COD)PtMe(acetone)$^+PF_6^-$ was indicated by the formation of the white precipitate of AgCl, which was removed by filtration leaving a clear colorless solution of the platinum complex. Upon addition of the red-orange solution of **I** in THF, the mixture immediately turned deep purple. The purple solid obtained from the mother liquor of this reaction gave an elemental analysis consistent with expectations of its formula shown above. In the mass spectrometer, a positive ion of m/z = 1522.9 corresponded to the cation [(1,5-COD)PtMe]$_2$[μ-$Mo_2(TiPB)_2(nic)_2$] less propene. The compound was only sparingly soluble in DMSO. The intense purple color arises from a strong absorption band centered at 560 nm, $\epsilon \approx 1 \times 10^4$ M^{-1} cm^{-1} (see Figure 5). Cyclic voltammetry and differential pulse voltammetry indicated a quasi reversible oxidation wave at −30 mV relative to the $Cp_2Fe^{0/+}$ couple in DMSO. This is close to the $\mathbf{I}^{0/+}$ couple and suggests that little positive charge has been transferred from the cationic platinum centers.

An attempt was made to prepare a molecular square, an analogue of the type of complex originally prepared by Stang, but where μ-$Mo_2(TiPB)_2(nic)_2$ substitutes for μ-4,4′-bipyridine. The complex (1,5-COD)$PtCl_2$ was allowed to react with $AgPF_6$ (2 equiv) in THF. Upon removal of the AgCl by filtration, a clear solution was obtained, which was then allowed to react with an orange solution of **I** in THF. This resulted in the formation of a fine blue precipitate that was insoluble in all common organic solvents. Its composition thus rests upon its elemental analysis. We cannot distinguish between the formation of a molecular triangle, a square or a polymeric structure. Only the deep blue color testifies to the coordination of **I** to the Pt^{2+} cations (see below).

Electronic Structure Calculations. To gain insight into the potential interactions between the metal atoms in the

(10) *Multiple Bonds Between Metal Atoms*, 3rd ed.; Cotton, F. A., Murillo, C. A., Walton, R. A., Eds.; Springer: New York, 2005.
(11) Bursten, B. E.; Chisholm, M. H.; Clark, R. J. H.; Firth, S.; Hadad, C. M.; Macintosh, A. M.; Wilson, P. J.; Woodward, P. M.; Zaleski, J. M. *J. Am. Chem. Soc.* **2002**, *124*, 3050.
(12) Clark, H. C.; Manzer, L. E. *J. Organomet. Chem.* **1973**, *59*, 411.

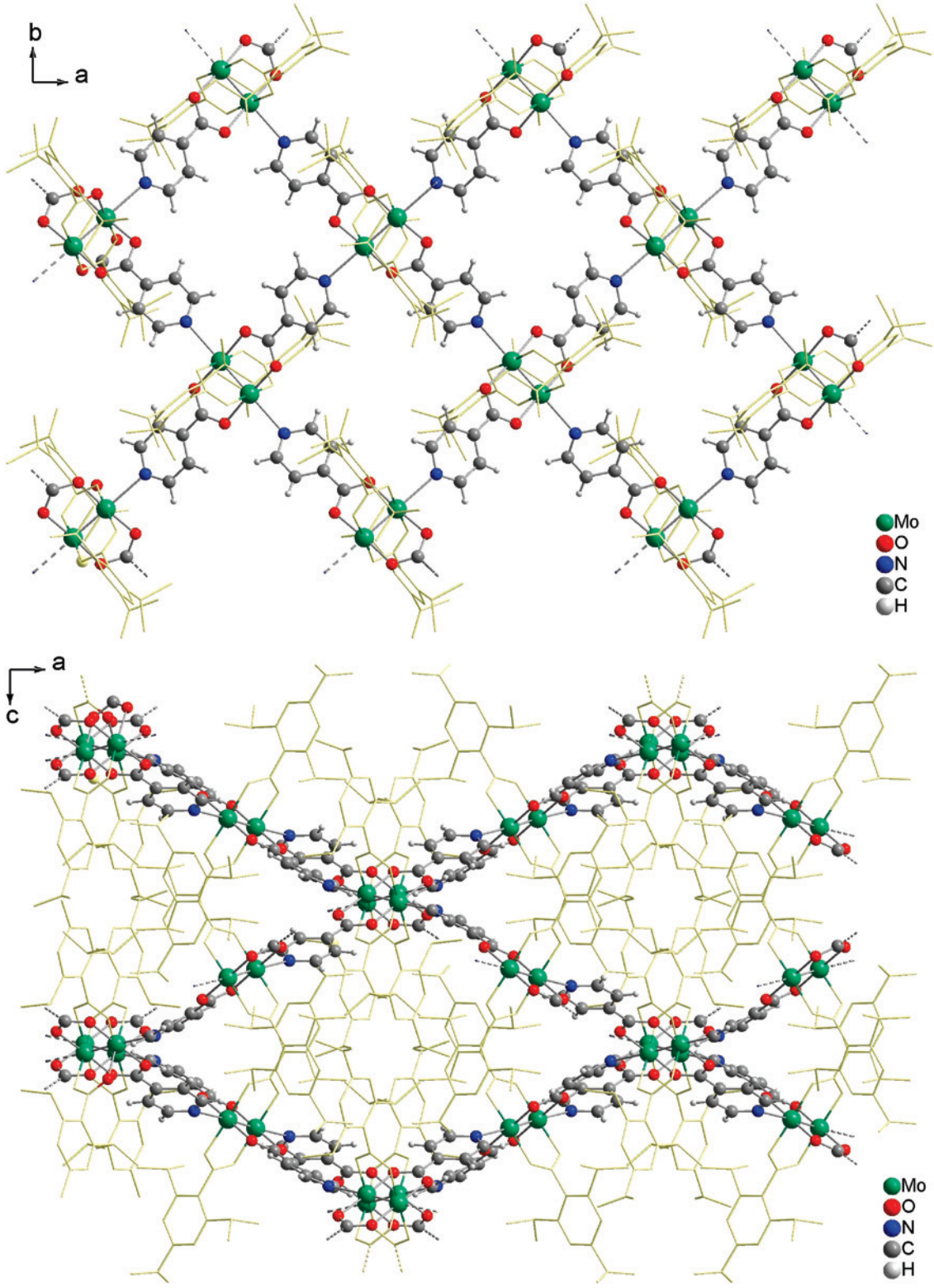

Figure 1. View along the *c*-axis (upper picture) and the *b*-axis (lower picture) of the crystal structure of **I**. The TiPB ligands are indicated as yellow frames for clarity.

extended chain compounds, we first carried out calculations on the model compounds *trans*-$Mo_2(O_2CH)_2(nic)_2$ (**I***), $[Mo_2(O_2CH)_3(nic)]_2\{\mu$-$Rh_2(O_2CH)_4\}$ (**II***-Mo_4Rh_2), $[Rh_2(O_2CH)_4]_2\{\mu$-$Mo_2(O_2CH)_2(nic)_2\}$ (**II***-Rh_4Mo_2), and $[Pt(COD)Me]_2\{\mu$-$Mo_2(O_2CH)_2(nic)_2\}^{2+}$ (**III***). These model compounds have formate ligands substituted for the triisopropylbenzoates bound to molybdenum and the acetates bound to rhodium. The platinum model compound **III*** was optimized in C_i symmetry; the other model compounds were all optimized in D_{2h} symmetry. Time-dependent density functional theory calculations were also carried out to assist in interpretation of the observed electronic absorption spectra.

For **I***, the calculations are in agreement with simple expectations. The HOMO is the $Mo_2\delta$ orbital, which interacts

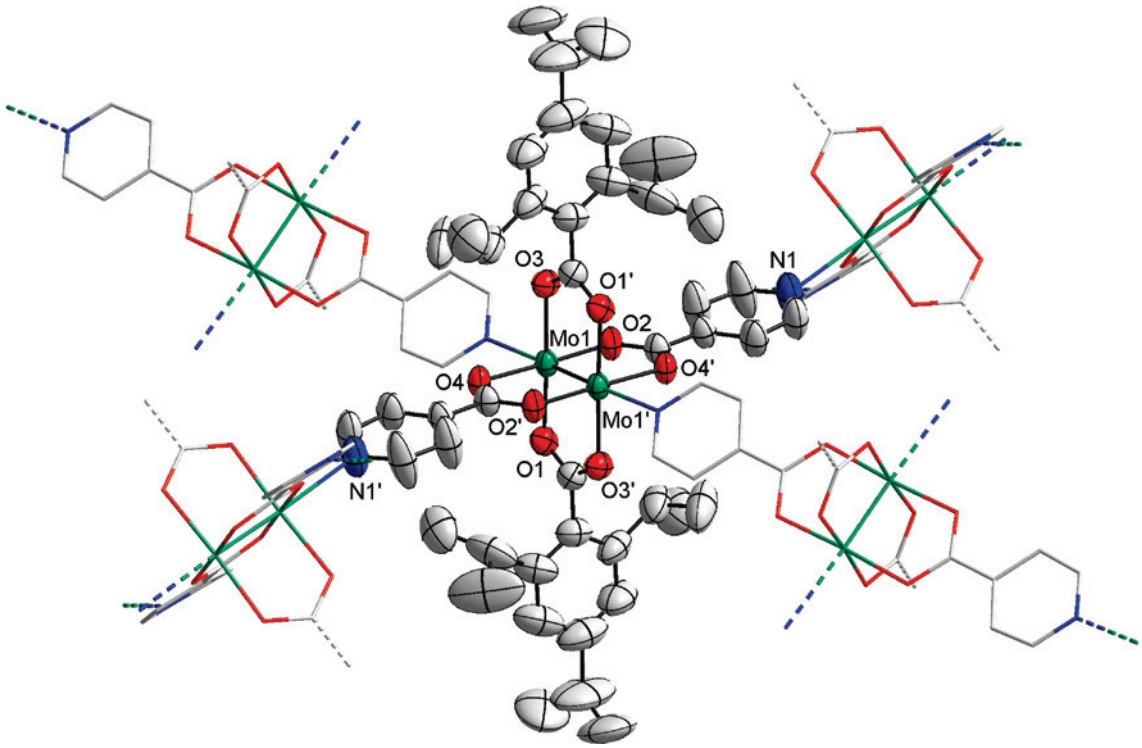

Figure 2. ORTEP drawing of **I** with anisotropic displacement parameters drawn at the 50% probability. Its 3-dimensional network structure is also indicated.

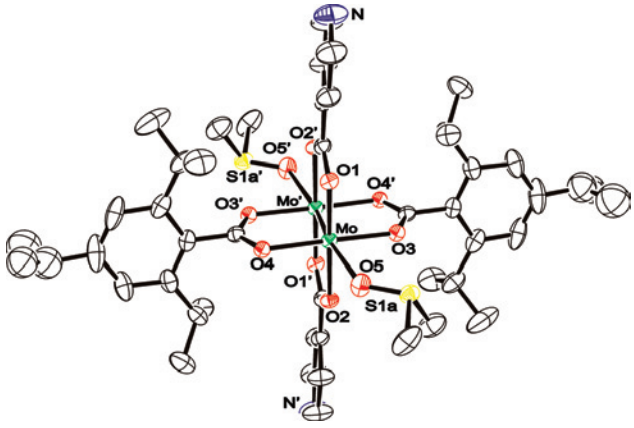

Figure 3. ORTEP drawing of the molecular structure of **I**$(DMSO)_2$ with anisotropic displacement parameters drawn at the 50% probability. Only one of the disordered sulfur atoms of the DMSO ligand is shown, and the hydrogen atoms are omitted for clarity. One half of the molecule is generated using a center of inversion. Mo−Mo′ = 2.1145(7) Å, Mo−O (carboxylate) = 2.11(1) Å (av), Mo−O5 = 2.490(3) Å.

weakly with the out-of-phase π^* combination of the two *trans*-4-isonicotinate ligands. The LUMO is the $Mo_2\delta^*$, which lies just below the LUMO+1 and +2, which are the in-phase and out-of-phase, respectively, π^* combinations of the isonicotinate ligands. The lowest energy intense electronic transition is the HOMO to LUMO+1, metal δ to isonicotinate charge transfer, calculated at 437 nm.

The calculated structure for the **II***-Rh_4Mo_2 model compound is given in Figure 6, alongside selected frontier MO plots. The calculated distances were Mo−Mo = 2.121 Å, Rh−Rh = 2.440 Å, and Rh−N = 2.179 Å. A summary of the calculated frontier molecular orbital energies is given in Table 2. The HOMO is predominantly $Mo_2\delta$ but with some admixture of in-phase $Rh_2\pi^*$, and its counterpart is the

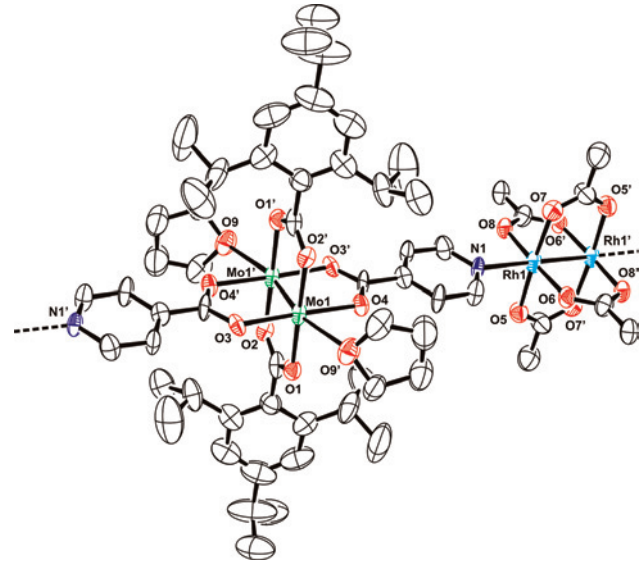

Figure 4. ORTEP drawing of the repeat unit in the coordination polymer **II**$(THF)_2$. Hydrogens have been omitted for clarity, and anisotropic displacement parameters are drawn at the 50% probability level. Both the Mo and Rh dimers sit on a crystallographic inversion center.

Table 1. Selected Bond Length (Å) and Angles (deg) for **II**

Mo1−O1	2.094(8)	Rh1−O5	2.032(8)
Mo1−O2′	2.109(8)	Rh1−O6	2.033(8)
Mo1−O3	2.124(8)	Rh1−O7	2.042(8)
Mo1−O4	2.132(8)	Rh1−O8	2.037(8)
Mo1−O9′	2.617(7)	Rh1−N1	2.219(9)
Mo1−Mo1′	2.109(1)	Rh1−Rh1′	2.397(1)
Mo1−Mo1′−O9′	167.8(2)	Rh1′−Rh1−N1	179.0(2)

HOMO−4, which is the out-of-phase $Rh_2\pi^*$ combined with some $Mo_2\delta$ character. The LUMO is the in-phase π^* combination of the isonicotinate ligands; the LUMO+1 is the $Mo_2\delta^*$, and the LUMO+2 the out-of-phase combination

Scheme 1

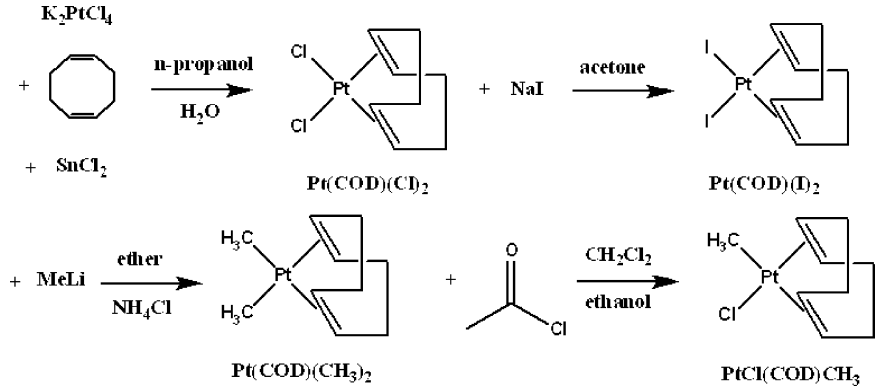

of the isonicotinate π^* which is mixed with the $Mo_2\delta$. The lowest energy fully allowed transition is calculated at 486 nm, with an oscillator strength of 0.85.

The calculated structure of the **II***-Mo_4Rh_2 model complex is shown in Figure 7, where Mo−Mo = 2.120 Å, Rh−Rh = 2.455 Å, and Rh−N = 2.275 Å. The energies of the frontier orbitals are given in Table 3. The HOMO is the out-of-phase combination of the $Mo_2\delta$ orbitals with an admixture of the $Rh_2\pi^*$. The HOMO-2 is the out-of-phase $Mo_2\delta$ combination with the $Rh_2\pi^*$. The LUMO and LUMO+1 are $Mo_2\delta^*$ combinations and the LUMO+2 an isonicotinate π^* combination. The lowest-energy intense electronic transition is calculated to be at 457 nm, a $Mo_2\delta$ to nicotinamate π^* MLCT, with an oscillator strength of 0.85. Selected Gausview plots of frontier orbitals are included in Figure 7.

The calculated structure of the $Pt_2Mo_2^{2+}$ containing cation, **III***, is displayed in Figure 8; Mo−Mo and Pt−N distances are 2.127 and 2.129 Å, respectively. The frontier molecular orbital energies are given in Table 4, with Gausview plots of selected orbitals shown in Figure 8. The HOMO is predominantly the $Mo_2\delta$ orbital and the LUMO is a π^* combination of the isonicotinate ligands with a significant contribution from the platinum $d_{x^2-y^2}$ that leads to the significant shift to lower energy of the $Mo_2\delta$ to nicotinamate π^* MLCT electronic transition. This transition is predicted to be at 577 nm with an oscillator strength of 0.80, which compares well with the observed spectrum shown in Figure 5.

Concluding Remarks. The title compound has been shown to be capable of acting as a bridging ligand in the construction of coordination polymers and as a ligand to bind to Pt(2+) centers. In the structure of **I**, we see the ambivalent nature of the molecule, which acts as both a donor and acceptor. In the structure of **II** and in its ligation to Pt(2+), it may be viewed as an inorganic analogue of the commonly employed 4,4′-bipyridine. The central $Mo_2(O_2C)_2$ core serves to extend this linkage by ~7 Å and couples the two C_5H_4N rings electronically via $Mo_2\delta-\pi$-conjugation. In contrast to 4,4′-bipyridine, the extended structure adopts a coplanar ground-state geometry thereby maximizing the influence of conjugation. The DFT calculations indicate that the 4-isonicotinate ligands do indeed serve to electronically couple the Mo_2 center to other metals. This is also evident from the low-energy electronic absorption spectrum of the $Pt_2Mo_2^{2+}$ containing compound **III**, in contrast to the parent compound **I**. Similarly, in other reactions involving Mo_2^{4+}, Ag^+, and Au^+ ions, intensely colored solutions are formed indicating significant electronic coupling to the Mo_2 center of **I** (see Supporting Information).

Further studies are in progress.

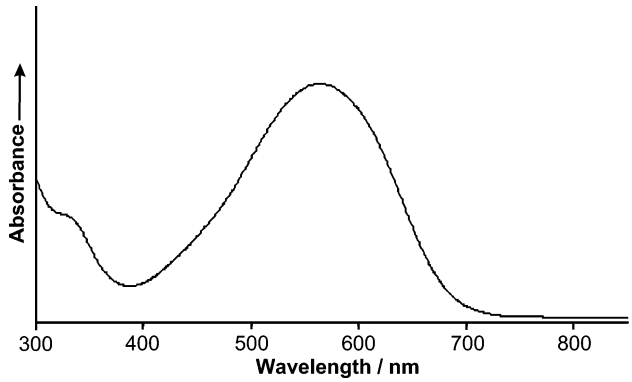

Figure 5. UV−vis spectrum of **III** in DMSO at room temperature.

Experimental Section

General Procedures. All reactions were carried out in an inert atmosphere using standard Schlenk line techniques and a nitrogen filled glovebox. Solvents were dried and distilled according to routine procedures. ^{1}H NMR data were recorded on a 250 MHz Bruker DPX Avance spectrometer or a 400 MHz Bruker DPX Avance spectrometer referenced to the solvent signal with chemical shifts reported in δ (ppm) and coupling constants reported in Hertz. Matrix-assisted laser desorption ionization time-of-flight (MALDI-TOF) data were collected on a Bruker Reflex III mass spectrometer, courtesy of the CCIC Mass Spectrometry and Proteomics Facility at The Ohio State University. This spectrometer was operated in linear, positive ion mode with a N_2 laser. The laser power was used at the threshold level necessary for the generation of a signal, and the accelerating voltage was set at 28 kV. A saturated solution of dithranol in THF was used as the matrix, which was layered over a sample spotted on the target plate. UV−vis spectra were recorded using a Perkin-Elmer Lambda 900 spectrometer. Both 1.00 and 2.00 mm quartz cells were used as indicated, and a spectrum of the neat solvent (THF or DMSO) was subtracted. Elemental analyses were performed at the Atlantic Microlab.

The cyclic voltammogram and differential pulse voltammogram of **III** were recorded using scan rates of 100 and 5 mV/s,

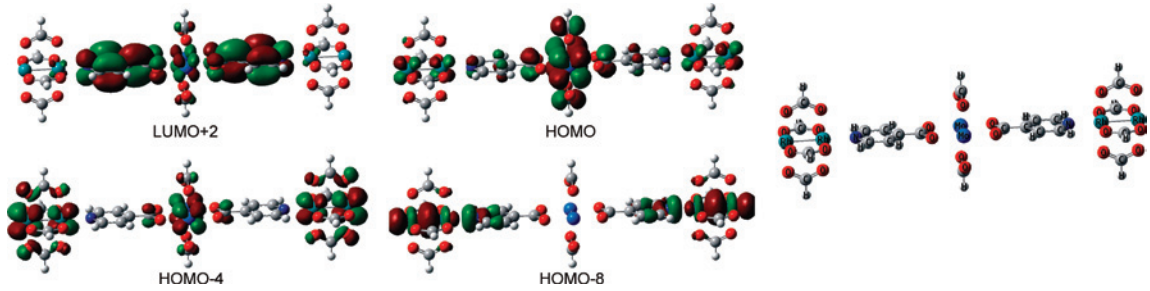

Figure 6. Calculated structure and selected frontier molecular orbital plots for **II***-Rh_4Mo_2. Orbitals are drawn at an isosurface value of 0.02.

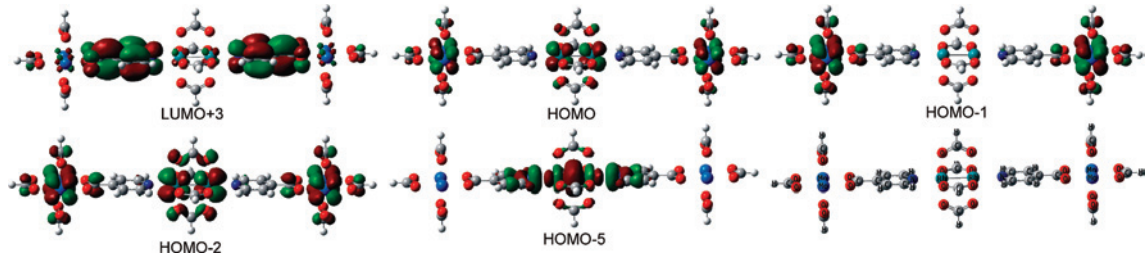

Figure 7. Calculated structure and selected frontier MO plots for **II***-Mo_4Rh_2 (orbitals drawn at an isosurface value of 0.02).

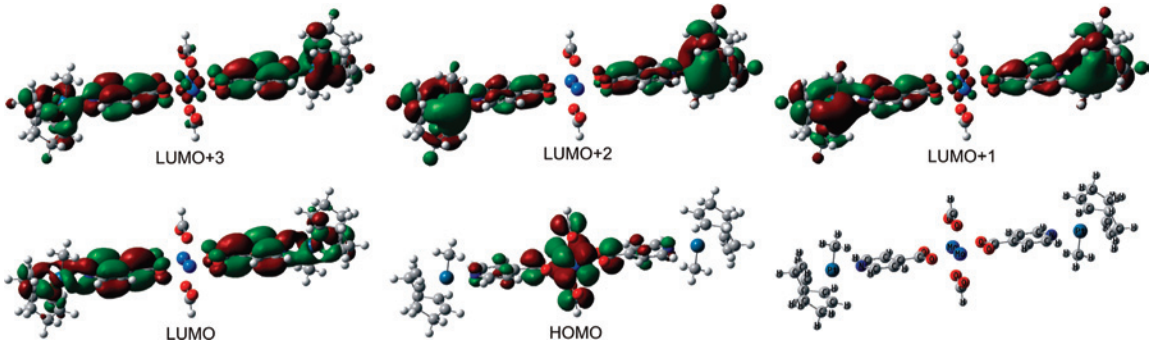

Figure 8. Selected frontier MO plots and calculated structure of **III*** (orbitals drawn at an isosurface value of 0.02).

Table 2. Calculated Frontier MO Energies and Assignments for **II***-Rh_4Mo_2

MO	energy (eV)	assignment	MO	energy (eV)	assignment
LUMO+2	−2.53	Nic π^*/Mo_2 δ	HOMO−5	−6.07	Rh_4 π^*
LUMO+1	−2.64	Mo_2 δ^*	HOMO−6	−6.07	Rh_4 π^*
LUMO	−2.85	Nic π^*	HOMO−7	−7.17	Rh_2 σ/N lone pair
HOMO	−5.86	Mo_2 δ/Rh_4 π^*	HOMO−8	−7.17	Rh_2 σ/N lone pair
HOMO−1	−6.03	Rh_4 δ^*	HOMO−9	−7.34	Rh_4 π
HOMO−2	−6.03	Rh_4 δ^*	HOMO−10	−7.34	Rh_4 π
HOMO−3	−6.03	Rh_4 in-phase π^*	HOMO−11	−7.41	Rh_4 π
HOMO−4	−6.06	Rh_4 out-of-phase π^*/Mo_2 δ	HOMO−12	−7.42	Rh_4 π

Table 3. Calculated Frontier MO Energies for the Mo_4Rh_2 Unit within the Chain

MO	energy (eV)	assignment	MO	energy (eV)	assignment
LUMO+3	−2.21	Nic out-of-phase π^*	HOMO−6	−6.81	Rh_2 π
LUMO+2	−2.23	Nic in-phase π^*	HOMO−7	−6.83	Rh_2 δ
LUMO+1	−2.25	Mo_4 out-of-phase δ^*	HOMO−8	−6.97	Rh_2 π
LUMO	−2.25	Mo_4 in-phase δ^*	HOMO−9	−7.16	Mo_4 out-of-phase π
HOMO	−5.45	Mo_4 out-of-phase δ/Rh_2 π^*	HOMO−10	−7.16	Mo_4 in-phase π
HOMO−1	−5.53	Mo_4 in-phase δ	HOMO−11	−7.17	Mo_4 out-of-phase π
HOMO−2	−5.62	Rh_2 π^*/Mo_4 out-of-phase δ	HOMO−12	−7.17	Mo_4 in-phase π
HOMO−3	−5.64	Rh_2 π^*	HOMO−13	−7.38	Mo_4 σ
HOMO−4	−5.65	Rh_2 δ *	HOMO−14	−7.38	Mo_4 σ
HOMO−5	−5.92	Rh_2 σ/in-phase N lone pair			

respectively. A Princeton Applied Research (PAR) 173 A potentiostat-galvanostat was utilized for electrochemical measurements, which was equipped with a PAR 176 current-to-voltage converter. All measurements were completed within an inert atmosphere in a 0.1 M solution of ^{n}Bu_4NPF_6 in DMSO. A single-compartment cell was used, which was equipped with a platinum working electrode, a platinum wire auxiliary electrode, and a pseudoreference electrode consisting of a silver wire in a 0.1 M ^{n}Bu_4NPF_6 solution in DMSO.

Table 4. Calculated Frontier MO Energies for $Pt_2Mo_2^{2+}$-Containing Molecule

MO	energy (eV)	assignment	MO	energy (eV)	assignment
LUMO+4	−6.88	Mo_2 δ^*	HOMO	−9.39	Mo_2 δ
LUMO+3	−6.56	Nic π^*/Pt $d_{x^2-y^2}$	HOMO−1	−10.94	Mo_2 π
LUMO+2	−6.10	Pt $d_{x^2-y^2}$/Nic π^*	HOMO−2	−11.01	Mo_2 π
LUMO+1	−5.50	Pt $d_{x^2-y^2}$/Nic π^*	HOMO−3	−11.06	Mo_2 σ
LUMO	−5.50	Nic π^*/Pt $d_{x^2-y^2}$	HOMO−4	−11.06	Pt d-orbital

Table 5. Crystallographic Data for **I**$(DMSO)_2$ and **II**$(THF)_2$·6THF

	I	I$(DMSO)_2$	**II**$(THF)_2$·6THF
formula	$C_{44}H_{54}Mo_2$ N_2O_8, (C_4H_8O)	$C_{48}H_{66}Mo_2$ $N_2O_{10}S_2$	$C_{52}H_{66}Mo_2$ $N_2O_{16}Rh_2$, $8(C_4H_8O)$
fw (g mol^{-1})	1002.88	1087.03	1949.60
T (K)	200	150(2)	123
λ (Å)	1.54178	0.71073	1.54178
cryst syst	tetragonal	triclinic	triclinic
space group	$I4_1/a$	$P\bar{1}$	$P\bar{1}$
a (Å)	27.5744(2)	10.206(1)	12.5330(7)
b (Å)	27.5744(2)	10.248(2)	13.2410(7)
c (Å)	14.7031(3)	13.932(2)	14.6756(6)
α (deg)	90	86.240(8)	94.455(4)
β (deg)	90	84.046(9)	99.593(4)
γ (deg)	90	62.388(6)	109.179(5
V (Å^3)	11 179.5(3)	1284.0(3)	2245.0(2)
Z	8	1	2
D_{calcd} (Mg m^{-3})	1.192	1.406	1.443
μ (mm^{-1})	4.053	0.625	5.753
R1/wR2 [$I > 2\sigma I$]	0.0414/0.1052	0.0452/0.1143	0.0815/0.2068
R1/wR2 [all data]	0.0555/0.1101	0.0601/0.1226	0.1223/0.2246

All values of potential have been referenced to the $FeCp_2^{0/+}$ couple, which was obtained upon addition of a crystal of $FeCp_2$ to the previous solution.

The following reagents were commercially available and were used without further purification: 2,4,6-triisopropylbenzoic acid, isonicotinic acid, potassium tetrachloroplatinate(II), 1,5-cyclooctadiene, sodium iodide, silver hexafluorophosphate, silver nitrate, dirhodium tetraacetate, and sodium tetraphenylborate. Silver tetraphenylborate was created through the metathesis of silver nitrate and sodium tetraphenylborate, followed by washing with hot deionized water to remove any remaining salts. $Mo_2(TiPB)_4$ was prepared following literature procedures,[13] as were $(COD)PtCl_2$[12] and (COD)PtCl(Me).[12]

Structural Determinations. X-ray crystallography data of **I**$(DMSO)_2$ were obtained using a Nonius Kappa CCD diffractometer and the data of **I** and **II**$(THF)_2$·6THF were obtained using a Oxford Diffraction Gemini Ultra diffractometer. The **I**$(DMSO)_2$ structure was solved by the Patterson method;[14] the **I** and **II**$(THF)_2$·6THF structures were solved by direct methods,[15] in SHELXS-97. Full-matrix least-squares refinements based on F^2 were performed in SHELXL-97 in the WinGX suite of programs with non-hydrogen atoms refined anisotropically.[14,16] All methyl hydrogens were included in the models at calculated positions using a riding model with $U(H) = 1.5U_{eq}$(bonded carbon atom). The rest of the hydrogen atoms were included in the model at calculated positions using a riding model with $U(H) = 1.2U_{eq}$(attached atom). Experimental data relating to the structure determination are displayed in Table 5.

Electronic Structure Calculations. The geometries of the model compounds were optimized in the gas-phase using density functional theory, as implemented in the Gaussian03 suite of programs.[17] The B3LYP functional[18−20] was employed along with the SDD energy consistent pseudopotentials[21] for molybdenum, rhodium, and platinum and the 6-31G* basis set[22] for O, N, C and H atoms. The geometry optimized structures were confirmed to be minima on their potential energy surfaces by vibrational frequency analysis. Electronic absorption spectra were calculated using the time-dependent DFT (TD-DFT) method.

Synthesis of $[Mo_2(TiPB)_2(nic)_2]$, I. A 250 mL Schlenk flask was charged with $Mo_2(TiPB)_4$ (1.0 g, 0.846 mmol) and isonicotinic acid (208 mg, 1.69 mmol). Ethanol (60 mL) was added, causing the reaction mixture to immediately turn bright red, and the mixture was stirred at room temperature for 4 days. The resulting red precipitate was isolated by filtration and washed with toluene (2 × 20 mL) and pentane (2 × 20 mL) before it was dried in vacuo. Yield: 740 mg (79.5%). ^{1}H NMR (400 MHz, DMSO-d_6, 27 °C, δ): 0.97 (d, $J_{HH} = 6.8$ Hz, 24H, isopropyl CH_3), 1.20 (d, $J_{HH} = 7.2$ Hz, 12 H, isopropyl CH_3), 2.85−2.91 (multiplet, $J_{HH} = 6.7$ Hz, 6H, aliphatic CH), 7.03 (s, 4H, TiPB aromatic CH), 8.11 (d, $J_{HH} = 6$ Hz, 4H, nic aromatic H), 8.95 (d, $J_{HH} = 6$ Hz, 4H, nic aromatic CH). MALDI-MS (THF sample): 930.8. UV−vis data (9.90×10^{-4} M THF solution, 1.00 mm cell): $\lambda_{max} = 474$ nm, $\varepsilon = 9.3 \times 10^3$ M^{-1} cm^{-1}.

Crystals of **I** were obtained from THF/CH_3CN solutions by layering with Et_2O, while crystals of **II**·2DMSO were obtained from saturated solutions.

Synthesis of $[\{Rh_2(O_2CMe)_4\}\{Mo_2(TiPB)_2(nic)_2\}]_\infty$, II. A blue-green solution of $Rh_2(O_2CMe)_4$ (9.5 mg, 0.021 mmol) in THF (6 mL) was added to an orange solution of **I** (20 mg, 0.021 mmol) in THF (6 mL) with stirring, resulting in the formation of a red precipitate. The red solid was isolated by decanting off the solvent, and then it was washed with 3 × 10 mL aliquots of THF. Axially coordinated THF molecules were removed by drying in vacuo at 60 °C for 8 h, giving an orange powder. Yield: 28 mg (95%).

(13) Cotton, F. A.; Daniels, L. M.; Hillard, E. A.; Murillo, C. A. *Inorg. Chem.* **2002**, *41*, 1639.
(14) Sheldrick, G. M. *Acta Crystallogr.* **2008**, *A64*, 112.
(15) Altomare, A.; Burla, M. C.; Camalli, M.; Cascarano, G. L.; Giacovazzo, C.; Guagliardi, A.; Moliterni, A. G. G.; Polidori, G.; Spagna, R. *J. Appl. Crystallogr.* **1999**, *32*, 115.
(16) Farrugia, L. J. *J. Appl. Crystallogr.* **1999**, *32*, 837.
(17) Frisch, M. J.; Trucks, G. W.; Schlegel, H. B.; Scuseria, G. E.; Robb, M. A.; Cheeseman, J. R.; Montgomery, J. A., Jr.; Vreven, T.; Kudin, K. N.; Burant, J. C.; Millam, J. M.; Iyengar, S. S.; Tomasi, J.; Barone, V.; Mennucci, B.; Cossi, M.; Scalmani, G.; Rega, N.; Petersson, G. A.; Nakatsuji, H.; Hada, M.; Ehara, M.; Toyota, K.; Fukuda, R.; Hasegawa, J.; Ishida, M.; Nakajima, T.; Honda, Y.; Kitao, O.; Nakai, H.; Klene, M.; Li, X.; Knox, J. E.; Hratchian, H. P.; Cross, J. B.; Bakken, V.; Adamo, C.; Jaramillo, J.; Gomperts, R.; Stratmann, R. E.; Yazyev, O.; Austin, A. J.; Cammi, R.; Pomelli, C.; Ochterski, J. W.; Ayala, P. Y.; Morokuma, K.; Voth, G. A.; Salvador, P.; Dannenberg, J. J.; Zakrzewski, V. G.; Dapprich, S.; Daniels, A. D.; Strain, M. C.; Farkas, O.; Malick, D. K.; Rabuck, A. D.; Raghavachari, K.; Foresman, J. B.; Ortiz, J. V.; Cui, Q.; Baboul, A. G.; Clifford, S.; Cioslowski, J.; Stefanov, B. B.; Liu, G.; Liashenko, A.; Piskorz, P.; Komaromi, I.; Martin, R. L.; Fox, D. J.; Keith, T.; Al-Laham, M. A.; Peng, C. Y.; Nanayakkara, A.; Challacombe, M.; Gill, P. M. W.; Johnson, B.; Chen, W.; Wong, M. W.; Gonzalez, C.; Pople, J. A. *Gaussian 03*, revision C.02; Gaussian, Inc.: Wallingford, CT, 2004.
(18) Becke, A. D. *Phys. Rev. A* **1988**, *38*, 3098.
(19) Becke, A. D. *J. Chem. Phys.* **1993**, *98*, 5648.
(20) Lee, C.; Yang, W.; Parr, R. G. *Phys. Rev. B: Condens. Matter* **1988**, *37*, 785.
(21) Andrae, D.; Haeussermann, U.; Dolg, M.; Stoll, H.; Preuss, H. *Theor. Chim. Acta* **1990**, *77*, 123.
(22) Hehre, W. J.; Radom, L.; Schleyer P. v. R.; Pople, J. A. *Ab Initio Molecular Orbital Theory*; John Wiley & Sons: New York, 1986.

Elemental analysis (%) calcd for $C_{52}H_{66}Mo_2N_2O_{16}Rh_2$: C, 45.50; H, 4.85; N, 2.04%. Found: C, 45.03; H, 5.06; N, 1.96%.

Synthesis of Crystals of II. A blue-green solution of $Rh_2(O_2CMe)_4$ (12 mg, 0.027 mmol) in THF (1.5 mL) and CH_3CN (1.5 mL) was layered over an orange solution of **I** (25 mg, 0.027 mmol) in THF (5 mL). Red to orange crystals start to grow in the area of the phase interface after two days. After 10 days, the still orange solution was decanted, and the crystals were washed with THF three times. Drying the crystals in vacuo for 2 h results in the formation of a red powder because of loss of interstitial THF molecules, but the THF molecules axially coordinated to the Mo_2^{4+} unit are retained. Yield: 25 mg (64%). Elemental analysis (%) calcd for $C_{60}H_{82}Mo_2N_2O_{18}Rh_2$: C, 47.50; H, 5.45; N, 1.85%. Found: C, 46.34; H, 5.44; N, 1.78%.

Synthesis of $[(1,5\text{-COD})PtMe]_2\{\mu\text{-}Mo_2(TiPB)_2(nic)_2\}(PF_6)_2$, III. Into a 100 mL Schlenk flask was added $PtCl(COD)CH_3$ (100 mg, 0.283 mmol), silver hexafluorophosphate (71.5 mg, 0.283 mmol), and THF (10 mL). This mixture was stirred and then filtered to remove the AgCl precipitate. To the clear, colorless filtrate $Mo_2(TiPB)_2(nic)_2$ (132 mg, 0.141 mmol) in THF (20 mL) was added dropwise. Upon addition, the reaction mixture immediately turned bright purple and was stirred for 11 days. The remaining solvent was removed in vacuo, and the resulting purple solid was washed with toluene (30 mL) before drying in vacuo. Yield: 195 mg (88%). ^{1}H NMR (DMSO-d_6, 250 MHz, 27 °C, δ): 0.79 (s, Pt-CH_3), 0.97 (d, 24H, isopropyl CH_3), 1.20 (d, 12H, isopropyl CH_3), 2.30 (m, cyclooctadiene CH_2), 2.82−2.92 (septet, 6H, isopropyl CH), 5.50 (m, cyclooctadiene CH), 7.04 (s, 4H, aromatic TiPB CH), 8.13 (d, 2H, nic CH), 8.35 (d, 2H, nic CH), 8.97 (d, 2H, nic CH), 9.14 (d, 2H, nic CH). MALDI-MS (DMSO sample): 930.1, 1204.0, 1522.9. UV−vis data (5.5×10^{-4} M DMSO solution, 2.00 mm cell): $\lambda_{max} = 560$ nm, $\varepsilon = 9.6 \times 10^3$ M^{-1} cm^{-1}. Elemental analysis (%) calcd for $C_{62}H_{78}N_2O_8P_2F_{12}Mo_2Pt_2$: C, 40.09%; H, 4.56%; N, 1.51%. Found: C, 39.56%; H, 4.64%; N, 1.68%. Electrochemistry: One quasi-reversible oxidation at −30 mV versus $Cp_2Fe^{0/+}$.

Reaction Between $Mo_2(TiPB)_2(nic)_2$ and $Pt(COD)Cl_2$. Into a 100 mL Schlenk flask was added $Pt(COD)Cl_2$ (100 mg, 0.267 mmol), silver hexafluorophosphate (135 mg, 0.534 mmol), and THF (10 mL). The mixture was stirred and then filtered to remove AgCl. The filtrate obtained was added to a solution of **I** (249.6 mg, 0.267 mmol) in THF (40 mL). A deep blue solution formed immediately, and after the mixture was stirred for 10 min, a blue solid began to form. Stirring was continued for 2 days, and the blue precipitate formed was isolated by filtration and washed with THF (5×20 mL) before it was dried in vacuo. The resulting solid was insoluble in all common organic solvents. Elemental analysis (%) calcd for $C_{208}H_{264}O_{32}N_8P_8F_{48}Mo_8Pt_4$: C, 40.98%; H, 4.37%; N, 1.84%. Found: C, 38.81%; H, 4.30%; N, 2.09%.

Acknowledgment. We thank the National Science Foundation and the Ohio Super Computer Center for support of this work at The Ohio State University, and F.D. thanks Studienstiftung des Deutschen Volkes for a doctoral fellowship at Universität Regensburg. N.J.P. gratefully acknowledges the Royal Society (London) for a University Research Fellowship.

Supporting Information Available: Crystallographic data for **I**, **I**$(DMSO)_2$ and **II**$(THF)_2\cdot$6THF. Pictures of vials showing the intense colors of reactions involving **I** as noted in the text. Atomic coordinates for the calculated structures noted in text as determined by DFT electronic structure calculations.This material is available free of charge via the Internet at http://pubs.acs.org.

IC800693R